The Fes tyrosine kinase guides CD19 receptor fate in B-cells by shaping regulatory Src phosphorylation networks

Helbig A.O.[1], Kofler M.[1,2], Gish G.[1], Lorenzen K.[1,4], Tucholska M.[1,5], Zhang C.[1], Roth F.P.[1,6,7,8], Colwill K.[1], Pawson T.[1†], Petsalaki E.[1,3,*]

[1]Lunenfeld-Tanenbaum Research Institute, Sinai Health Systems, 600 University Ave, M5G 1X5, Toronto, Canada

[2]Keenan Centre for Biomedical Research, 209 Victoria Street, M5B 1T8, Toronto Canada

[3]European Molecular Biology Laboratory - European Bioinformatics Institute, Wellcome Genome Campus, Hinxton, CB10 1SD, United Kingdom

[4]European XFEL GmbH, Holzkoppel 4, 22869, Schenefeld, Germany

[5] Sanofi Pasteur, 755 Steeles Ave W, M2R 3T4, Toronto, Canada

[6]Donnelly Center and Departments of Molecular Genetics and Computer Science, University of Toronto, Toronto, Ontario, M5G 1X8

[7]Center for Cancer Systems Biology, Dana-Farber Cancer Institute, Boston, Massachusetts, 02215, USA

[8]Canadian Institute for Advanced Research, Toronto, Ontario, M5G 1Z8, Canada

[9]Lead Contact

[†]deceased

*Correspondence: petsalaki@ebi.ac.uk

Summary

The c-Fes protein tyrosine kinase is a proto-oncogene that can also act as a tumor suppressor. We implemented a novel phosphoproteomics-based analysis that establishes cognate kinase-substrate associations, and revealed that c-Fes directly phosphorylates Dok1, Ptpn18 and Sts1, facilitating recruitment of the Src inhibitory kinase Csk to these substrates. These interactions resulted in modulation of Src signaling following B-cell receptor (BCR) stimulation and subsequent alteration of the protein levels of CD19, a membrane-localized BCR co-receptor and emerging key protein affecting the development of B- and plasma cell-lymphoma. Strikingly, manipulating c-Fes expression levels drove opposing biological outcomes; low-level exogenous c-Fes expression led to a strong increase in CD19

protein levels while high c-Fes expression abolished CD19 protein levels. Thus, we propose that a balance of c-Fes and Src signaling can regulate maintenance of CD19, which may influence cellular outcome of accelerated hematopoietic tumorigenesis or tumor suppression.

Keywords

Phosphoproteomics, Functional signaling networks, Mass spectrometry, Soluble tyrosine kinases, Systems biology, B-cell regulation, Cancer biology

Introduction

Over the last 20 years, studies on the cytoplasmic tyrosine kinase Fes and the related kinase Fer have provided key insights into kinase structure and general protein domain architecture, particularly the discovery of the non-catalytic phosphotyrosine binding SH2 domain (*1*), (*2*). Fes and Fer share a unique domain composition: A N-terminal F-BAR domain, a central SH2 domain, and a C-terminal tyrosine kinase domain. F-BAR domains interact with phosphoinositides to promote membrane localization and invagination (*3*), (*4*), while the phosphotyrosine binding SH2-domains propagate cellular information processing by coupling localization and activation of these soluble tyrosine kinases. Although molecular functions have been ascribed to its individual domains, Fes's role in cell signaling is still poorly understood. Only a few Fes substrates such as STATs, CTTN and Bcr have been identified so far (*5*), and little is known about how this kinase's phosphorylation events influence cellular function.

c-Fes knockout macrophages display immune hypersensitivity which points to Fes being involved in the regulation of the immune response (*6*). Indeed, Fes is highly expressed in the myeloid system where it induces the differentiation of myeloid progenitor cells into terminal macrophages (*7*), (*8*). It is also

expressed in several other lymphoma lines and blood tissues (*9*) suggesting that Fes is active in multiple lineages of the hematopoietic system. Fes, along with Fer, is activated downstream of oncogenic KIT receptors in primary acute myeloid leukemia (AML) and is expressed in AML cell lines, where it is necessary for cell proliferation and survival (*10*).

This activating role of Fes in AML contrasts with its apparent role as a tumor suppressor in colorectal cancer (*11*), (*12*), and underscores the need for a better understanding of Fes-modulated signaling networks. Particularly, a detailed grasp of *in-vivo* substrates is necessary to link such observations to a molecular basis. Therefore, a systems biology approach, providing comprehensive information on direct substrates and their operation within the signaling network is crucial to place Fes into a more defined functional context. Therefore, we employed a systems biology approach to define the functional role of Fes in the B-cell line DG75. We utilized quantitative phosphoproteomics and bioinformatics, to identify a set of direct *in-vivo* substrates and studied how these substrates operated within the B-cell receptor-signaling network. This rich resource of system wide kinase-substrate associations advanced our understanding of the biological role of the Fes kinase and shades light on how the kinase could possibly suppress and promote different cancers, respectively.

Results

Fes activation and selectivity in B-cells

To better understand signaling pathways influenced by the Fes kinase, we sought a biological process where catalytic activity could be induced by the application of biological stimulus. Focusing on the hematopoietic system where there is evidence for Fes activity (*13*), we tested the expression of Fes in the RAW 264.7 macrophage cell line as a representative of the myeloid system and in the human B-

lymphocyte cell line DG75 as a model for the lymphoid system. Since the abundance of Fes in DG75 cells was relatively low, compared to RAW 264.7 macrophages (Figure S1A), we chose to conduct further experiments in DG75 cells. Here, we could effectively induce Fes signaling by exogenous Fes kinase expression and receptor stimulation, a strategy that would be much less effective in myeloid model systems already containing a high baseline of endogenous Fes signaling. Immunofluorescence microscopy indicated that endogenous Fes co-localizes with the B-cell Receptor (BCR) in resting DG75 cells (Figure 1A). Further analysis to evaluate the model system indicated that DG75 cells indeed bear hallmarks of B-cell signaling including expression of B-cell markers (CD19) and activation of downstream signaling pathway components (Lyn, Syk, Btk, Akt, Erk) after BCR stimulation through IgM (Figure 1B, Figure S1B-D). IgM stimulation led to phosphorylation of endogenous Fes of its activating site Y713 (Figure 1C). The Fes specific small molecule inhibitor TAE684 (*14*) effectively inhibited the pY713 signal, suggesting the site to be auto-phosphorylated. IgM stimulation also activated stably expressed GFP-tagged full-length Fes or a catalytically active SH2-kinase fragment in DG75 cells as measured by MRM mass spectrometric analysis of the Y713 auto-phosphorylation (Figure 1D). Curiously, a stronger pY713 signal was observed for the full-length F-BAR domain-containing protein than the truncated Fes derivative following stimulation in cells. To determine the extent to which the F-BAR domain contributes to kinase function, we performed an *in-vitro* substrate phosphorylation analysis by applying a broad-spectrum kinase inhibitor (FSBA) to DG75 cell lysate then incubating the kinase-dead lysate with purified full-length Fes or SH2-kinase. The added kinases amounts were normalized on kinase activity of the recombinant proteins since the SH2-kinase protein displayed much higher activity that the full length kinase *in-vitro* (data not shown). As detected by an anti-phosphotyrosine antibody (4G10) immunoblot, the exogenous Fes kinases were observed at the expected molecular weight (Figure 1E). The number of phosphorylated target proteins was lower for the F-BAR containing full-length Fes even though the level of activity, as measured by auto-phosphorylation level for full length and truncated kinases was comparable. This indicates that the F-BAR domain plays an integral part in establishing substrate specificity as well as enabling kinase activation following BCR stimulation.

Fes signaling within the B-cell phosphotyrosine network

To analyze Fes signaling downstream of BCR activation, we implemented a phosphoproteomics-centered strategy. We first manipulated Fes activity through stable or transient expression of c-Fes or an activated Fes kinase E708A (Figure S2) to define direct Fes substrates and highlight its influence within the global signaling network (Figure 2A). Second, the BCR of DG75 cells was activated using anti-human IgM to establish a global picture of BCR-related signaling, both in the context of endogenous and over-expressed Fes. Third, we inhibited endogenous Fes, Src, or MEK using the specific inhibitors TAE684, PP2, SrcI1, and PD184352, respectively, to establish signaling direction and topology. We employed a protocol that maximized phosphoproteome capture through TiO_2 enrichment of phosphorylated tryptic peptides followed by strong cation exchange (SCX) chromatography or immunoprecipitation of tyrosine phosphorylated peptides prior to mass spectrometry analysis. Dimethyl chemical labeling was utilized to compare three individual samples in one MS experiment (Figure 2B).

This global signaling analysis identified quantitatively 33,207 unique phosphorylated peptides from 5,518 proteins corresponding to 27,143 individual phosphorylation sites (Table S1). A greater than three-fold change in dimethyl isotope ratio, indicating significant abundance change, was observed for 4,890 peptides (from 1,992 proteins). All acquired quantitative ratio data from the 13 large-scale experiments was pooled and analyzed using SELPHI (*15*) to uncover kinase to substrate dependencies and associations. The SELPHI pipeline scores potential kinase-substrate connections based upon a correlation of the level of kinase phosphorylation to the level of phosphorylation on potential substrates in various experimental conditions assuming a linear relationship. 693 associations were extracted using SELPHI from the 1742 unique tyrosine phosphorylation sites identified by MaxQuant. The most confident connections between activating sites on tyrosine kinases and potential substrates are shown in Figure 2C and Table S2. This approach confirmed Syk and the Src family kinase Lyn as major hubs in the BCR

signaling network, consistent with the current literature (*16*). Many assigned substrate sites were associated with multiple kinases throughout the different perturbations of the BCR signaling network designed to dissect the network topology. Such apparent redundancies, as seen for example in shared substrate pools for Lck and Tec (Figure 2C), might be important factors that, on one hand, grant signaling networks a high degree of plasticity and adaptability and, on the other hand, make signaling pathways robust to stochastic background activation. Additionally, enrichment of serine/threonine phosphorylated peptides enabled us to calculate SELPHI connections between serine/threonine kinases and potential downstream substrate sites (Figure S3 and Table S3). Thus, the perturbation of different signaling components using kinase inhibitors and exogenous Fes kinase expression allowed us to establish global kinase-substrate relationships and extract a potential substrate catalogue for the endogenous Fes kinase for subsequent verification.

Thirteen potential substrate sites showed a high correlation to Fes activation: Syk (Y352, Y525), Lyn (Y397), Blk (Y389), Tec (Y519), Mapk1, Stam2 Swap70 (pY517), Dok1 pY489, Pik3ap1 pY694, Nck1 pY105, Sts1 pY19, Ptpn18 pY389 (Figure 3B, in red). A kinase assay was developed using a 13-mer peptide spots array of 100 potential tyrosine sites that included those 13 potential Fes substrate sites plus an additional 87 sites predicted from the SELPHI to be phosphorylated by other kinases. The known Fes substrate Cttn as well as the Fes auto-phosphorylation site were included as positive controls (Figure 3A, Table S4). The assays were carried out using both soluble SH2-kinase and isolated kinase domain to test for effects of the SH2-domain on substrate specificity. Similar phosphorylation patterns and Fes substrate consensus sequences were observed for both constructs (Figure 3A) with 11 of the 13 SELPHI-predicted Fes substrate sites phosphorylated *in-vitro* (Mapk1 Y187 and Stam2 Y374 were not confirmed as Fes substrates) (Figure 3B). Notably, many of the 87 non-Fes mediated target sites from the SELPHI analysis (34 sites for the SH2-kinase and 51 sites for the kinase construct) we detected phosphorylation by Fes *in-vitro*. This highlights the need to employ complementary *in-vivo* and *in-vitro* approaches to reduce false positive kinase-substrate associations. Thus, our analysis showed that Fes can readily phosphorylate the

activation loops of Syk (Y352, Y525), Lyn (Y397), Blk (Y389) and Tec (Y519) and thereby activated these tyrosine kinases. (Figure 3B). In addition to Fes and these 4 direct tyrosine kinase substrates Syk, Lyn, Blk and Tec, 6 other soluble tyrosine kinases (Fgr, Sgk223, Lck, Abl2, Btk and Tnk2) displayed increased phosphorylation after BCR cross-linking (Figure 3C). From this set of activated tyrosine kinases, the signal further propagated towards serine/threonine specific MAP kinases. Tyrosine phosphorylation of pY187 and pY204 partially activates Mapk1 and Mapk3 respectively (*17*). Our SELPHI and peptide array data suggests that Fes does not phosphorylate these components directly, but instead influences mitogenic signaling indirectly through activation of Blk, Syk, Lyn and Tec (Figure 3D). The SELPHI correlation analysis of the data predicts further connections to serine/threonine kinases such as Chek1 and Gsk3b and, importantly, includes previously established kinase connections such as Mapk1 to Rps6ka1 (*18*), providing further credence that this phosphoproteomics strategy successfully assembled a directional signaling network. Connecting Fes activity to this extensive network context directed further detailed and mechanistic studies of its influence on B-cell regulation.

Fes phosphorylation recruits the tyrosine kinase Csk into distinct signaling complexes

Apart from tyrosine kinases, direct Fes substrates also included the guanine exchange factor Swap70 (pY517), various adaptor proteins (Dok1 pY489, Pik3ap1 pY694 and Nck1 pY105) and tyrosine phosphatases (Sts1 pY19 and Ptpn18 pY389) (Figure 3B, E). The phosphorylation sites in Dok1, Sts1 and Ptpn18, comprised the sequence pattern LYSxV, which resembled the overall Fes phosphorylation motif LYExV from our peptide array data. This prompted us to further investigate these substrates. To confirm direct Fes-mediated phosphorylation of these specific sites in the context of full-length proteins, we expressed GFP-tagged WT Dok1, Ptpn18 and Sts1 or tyrosine to phenylalanine mutants of this motif in HEK293T cells, and performed *in-vitro* phosphorylation assays on the immunoprecipitated substrates using purified Fes SH2-kinase. All three proteins could be phosphorylated by Fes *in-vitro* as detected by

western blotting using anti-phosphotyrosine antibody 4G10 (Figure 3F). While phosphorylation of Dok1 and Sts1 was strongly reduced by the Y/F mutations, there was no clear difference between WT and Y389F mutant Ptpn18 suggesting the presence of multiple *in-vitro* phosphorylation sites for Fes.

The functional consequences of tyrosine phosphorylation of Dok1, Sts1, and Ptpn18 on their LYSxV motifs are unknown. Therefore, we tested whether these phosphorylation sites further propagated the BCR signaling through the modulation of interactions of Dok1, Sts1, or Ptpn18 with other cellular components. We expressed the proteins in DG75 cells together with the activated Fes E708A kinase mutant to drive robust, BCR dependent phosphorylation. In parallel, we co-expressed the Y/F mutants with Fes E708A kinase. Interacting proteins were then identified by IP/MS (Figure 4A and Table S5). This analysis revealed that the C-terminal Src kinase (Csk) was recruited to this motif in a Fes-dependent manner as it was only seen in immunoprecipitates with WT Dok1, Sts1, and Ptpn18 and absent in the Y/F mutants. This recruitment is consistent with recent reports (Brehme, 2009, Davidson 2016). The Fes-specific inhibitor TAE684 effectively blocked phosphorylation of these sites during BCR stimulation experiments in WT DG75 cells (Figure 4B). These interactions were likely mediated by Csk's SH2 domain that recognizes pTyr motifs of the type pY(A/T)(K/R/Q/N)(I/V/M) (*19*) also found in the LYSxV phosphorylation sites. Moreover, phosphorylation-mediated Csk recruitment was Fes-specific: co-expression of Ptpn18 with Fes in Hek293T cells robustly increased the interaction between Ptpn18 and endogenous Csk, consistent with direct substrate connection of Fes with Ptpn18, while co-expression of Ptpn18 with Src kinase yielded a much lower association. Abolishing Ptpn18 phosphatase activity (C228/S) did not have an effect on Csk recruitment (Figure 4C).

Co-expression experiments of Csk and Ptpn18 further confirmed that the YF mutation disrupted the interaction between these two proteins (Figure 4D). Interestingly, Csk binding correlated with tyrosine phosphorylation of Ptpn18. Given the activation of Csk by SH2-ligand binding, it is plausible that the

increased Csk levels drove association with sporadically phosphorylated Ptpn18 and consequently fostered further phosphorylation. This could explain how Fes induced phosphorylation could activate Csk by a recruitment mechanism, further propagating signaling events.

Fes signaling regulates CD19 levels via its substrate Sts1

Following the observation that the Fes kinase co-localizes with the BCR and activates following BCR stimulation (Figure 1), we mined published BCR interaction data using the STRING website. This showed that the interactome of the Fes substrate Sts1 ties to the BCR complex (CD79A, CD79B and CD19) via the E3 ubiquitin ligase Cbl (Figure 5A). CD19 plays a decisive role in B-cell activation as it lowers the threshold for the initiation of the signaling response upon exposure to an antigen. A productive receptor engagement will lead to CD19 phosphorylation on cytoplasmic tyrosine residues including Y531 which serves as docking sites for the regulatory subunit p85 of PI3K (*20*), (*21*). Titration of WT Fes kinase into DG75 cells revealed that low-level expression of exogenous Fes increased endogenous CD19 protein levels while stronger overexpression reduced them. (Figure 5B). Interestingly, Src phosphorylation at Y527 paralleled the observed changes in CD19 levels. Since this site in Src is directly phosphorylated by Csk in cells (*22*) and leads to its inactivation, Src activity might be implicated in the down-regulation of CD19. Again, this effect of Fes on CD19 expression was specific, as a similar expression experiment using Tec kinase did not affect CD19 levels. Consistently, exogenously Src expressed at various levels also did not alter CD19 levels. (Figure 5B).

Since we identified Sts1, Dok1 and Ptp18 as Fes substrate proteins that mediate Csk recruitment, we also tested their ability to modulate CD19 levels. We ectopically expressed WT or the Y/F mutants and monitored their impact on CD19 levels (Figure 5C). Only Sts1 displayed a difference related to the Fes substrate site as the WT protein generated higher CD19 levels than the mutant did. To monitor for an effect on CD19 function in coordinating downstream PI3 kinase and Src signaling pathways, we also

measured phosphorylation on Tyr531 of CD19 using a phospho-specific antibody (Figure 5C). While differences in signal were observed, they paralleled those seen for CD19 levels. This indicates that the Fes-mediated Sts1 phosphorylation modulates the magnitude of the B-cell response by altering the overall level of the CD19 protein. Expression of Sts1 Y19F, which fails to recruit Csk, did not produce this effect, highlighting the mechanistic connection of Fes, Csk and Sts1. Our interaction map showed that Sts1 is constitutively associated with Cbl and Cblb and upon BCR stimulation, this signaling complex is recruited to various adaptor molecules such as Grb2, Shc1 and notably Pik3ap1 (Figure 4A), which acts, together with CD19, as a scaffold for PI3K (*20*). Although the exact mechanism is still to be determined, we suggest that Fes is modulating CD19 expression levels, at least in part, through the concerted efforts of the Fes-Csk-Sts1 complex opposing Cbl-mediated degradation. (Figure 5D).

Discussion

The evolution of tyrosine kinases and phosphatases coincided with the emergence of multi-cellularity and the advent of complex life (*23*). Such a paradigm shift however can apparently not be achieved without downsides. Exerting profound influence on cell proliferation and metabolism, many tyrosine kinases such as Src and Abl have been shown to carry oncogenic potential (*24*)(*25*), requiring tight inhibitory feedback mechanisms (*26*). Therefore, a better understanding of the intricacies of tyrosine phosphorylation networks and their regulatory mechanisms is of outmost importance to understand their subsequent translation into phenotypic outcomes or, in aberrant situations, into uncontrolled cell growth and associated diseases such as cancer. To this end, we dissected the B-cell signalling architecture to identify the substrate spectrum and regulatory network surrounding the Fes tyrosine kinase.

Fes signaling involves localization and SH2-/Kinase-domain cooperativity

Antigen binding to the BCR induces clustering of the receptor into lipid rafts (*27*) and facilitates the downstream signaling cascade. The Fes F-bar domain seems to be the driving force for Fes membrane localization (*4*) and we demonstrate that it also affects substrate selectivity. The decrease in Fes activation *in vivo*, when the F-bar domain is deleted, points to membrane localization being a critical factor for signal transduction to Fes after BCR clustering. Hypothetically, membrane rearrangement during BCR clustering could concentrate BCR-associated Fes kinase into signaling environments leading to its auto-phosphorylation and activation. This then in turn leads to phosphorylation of Fes substrates such as membrane-associated tyrosine kinases (e.g. Syk, Lyn), phosphatases (Ptpn18, Sts1) and adaptor proteins such as Dok1, that further direct cellular outcome. The SH2 domain was originally defined in Fes as a non-catalytic region contributing to the catalytic activity of the neighboring kinase domain (*1*) with whom it forms a stable complex (*28*) (*29*). Interestingly, our identified consensus sequence for Fes kinase specificity matches the Fes SH2-binding specificity (YEXVX) as determined previously (*30*). The SH2 domain links phosphotyrosine binding of primed targets to catalytic activation (*30*). Shared motif specificity of the SH2 and kinase domain for the same sites might lead to distinct signal amplification by increasing kinase concentration in a particular cellular microenvironment with highly abundant substrate through a synergistic effect of phosphorylation and localization. In this regard, it has been demonstrated that Dok1 and Sts1 can form oligomers in cells (*31*), (*32*) underlining a possibility of signal amplification through overlapping of kinase- and SH2-domain specificity.

We demonstrated that Fes phosphorylation in B-lymphocytes of Dok1, Sts1, and Ptpn18 recruits the Csk tyrosine kinase. Csk is not primarily regulated by phosphorylation; instead it seems to be dominantly spatially controlled (*33*) by phosphorylation-based recruiting via its SH2 domain which simultaneously activates the kinase domain (*34*). Our data indicates that the Csk kinase- and SH2-domain specificity have evolved to complement each other by amplifying phosphorylation of the protein it was shown to bind (Figure 4A/4D). *In-vitro* determination of SH2-domain specificity also found similar consensus motifs for Csk and Fes SH2-domain binding (*35*). This highlights again the close association between those two

protein domains in the regulation of signaling circuits. Taken together, our results point to a model where Csk localization is initiated by Fes phosphorylation on specific protein complexes and amplified by the SH2- and kinase-domains of both kinases. Consecutively, this would lead to a spatially and temporally controlled, localized Src inactivation within specific protein complexes in the cell.

The Fes kinase – tumor suppressor or oncogene?

Our SELPHI analysis showed that Fes is able to activate downstream mitogenic kinases such as Mapk1/3 through signal propagation, which might contribute to its oncogenic potential in various cellular contexts. However, our experiments also point to Fes's involvement in the modulation of the critical decision process around Src activation and inhibition. We show that Fes signaling plays a crucial role in tuning and altering Src family kinases *in-vivo* by directly activating Lyn kinase through phosphorylation at the activation loop and indirectly contributing to Src family inhibition through Csk. Indeed, titration of Fes expression levels indicated that Fes activity is critical to tip the scales of Src regulation via Csk recruitment in either direction, which may contribute to the resulting modulation in CD19 levels that we concomitantly observed (Figure 5B). These different roles in signal propagation possibly explain Fes' seemingly paradox functions in cancer.

Sts1, a ubiquitin-binding tyrosine phosphatase, has been implicated in counteracting Cbl-mediated receptor degradation through the dephosphorylation of target sites for the Cbl SH2 domain that guide the receptor ubiquitination and degradation process (*31*) (*36*). Typically, these sites are Src targets (*37*) and it is conceivable that Csk recruitment to Sts1 signaling complexes is needed to locally inhibit Src activity in cooperation with the Sts1 dephosphorylation of Src target proteins to facilitate its function. Additionally, it has been demonstrated that CD19 can form a complex with Cbl, down-regulating activated CD19-PI3K complexes (*38*). We found that the Csk-recruitment site on Sts1 generated by Fes phosphorylation is necessary for Sts1 function of stabilizing CD19, possibly by opposing Cbl function. According to this

observation, localized Src inhibition via Csk recruitment, as well as Sts1 tyrosine phosphatase activity, act in concert to achieve effective Cbl opposition and maintain CD19 levels (Figure 5B/C). Previous data on enforced CD19 expression showed that, despite its function to balance the B-lymphocyte signaling threshold, CD19 also leads to growth retardation of malignant plasma cells (Multiple myeloma) (*39*) and thus can act as a tumor suppressor in the lymphoid system. As such, it is an important factor in lymphoid malignancies since CD19 loss is often observed in Multiple myeloma cancerous cells (*40*), (*41*). Our data indicates that low Fes expression levels in lymphocytes might constitute a signaling threshold where Fes-mediated Csk recruitment contributes to high CD19 levels, helping to safeguard lymphocytes from tumorigenic degeneration. Interestingly, rising Fes kinase ectopic expression levels can also have an opposite compensation effect, strongly reducing CD19 levels. This observation might provide a novel angle for therapeutic strategies targeting Fes using kinase inhibitors to reverse such repressive effects on CD19 in plasma cell cancers. In support of this, an RNAi screen demonstrated Fes to be an important driver of Multiple myeloma cell survival (*42*).

By lowering CD19 levels, Fes might contribute to an oncogenic phenotype when expressed at high levels in plasma cells but its ability to control Csk recruitment could be a means to counteract oncogenic Src signaling in other tissues. This might be especially pronounced in colon cancer where aberrant Src signaling has been detected in about 80% of the cases (*43*) and where Fes has been identified as a tumor suppressor. Additionally, it has been shown that Src can prime the adaptor Shc1 for EGFR mediated phosphorylation thus activating the Ras-MAPK pathway (*44*). In such a molecular context, it is conceivable that Fes expression might indeed help to counteract oncogenic Src and thus the Fes kinase could operate as a tumor suppressor.

In summary, we presented a systems biology approach to address the enigmatic biological role of the Fes kinase in the B-cell line DG75. We report that Fes is able to intricately modulate Src signaling, recruiting the Src inhibitory kinase Csk to multiple signaling complexes in lymphocytes. We observed that this mechanism controls the protein levels of the CD19 co-receptor, at least in part, via the Fes substrate Sts1. We propose that, through dysregulation of these mechanisms, Fes could potentially contribute to oncogenic effects in the lymphoid system especially in specific cancers such as CD19-deficient lymphomas.

Methods

Cell culture, transformation and stimulation

The DG75 human lymphoblast cell line and the mouse macrophage RAW264.7 cell line were obtained from American Type Culture Collection (ATCC). DG75 cells were cultured at 37°C, 5% CO_2 in RPMI with glutamate/Pen-Strep supplemented with 10% fetal bovine serum (FBS). For transfection, cells were grown to a density of $0.7x10^6$ and washed 3 times in RPMI. 20ug of plasmid DNA was mixed with 10^7 cells in 0.5ml of RPMI. Cells were incubated for 10 minutes and electroporated (BTX Electro Square Porator ECM 830) by three 8ms pulses at 225V in a 4mm cuvette. After 10 minutes of incubation, cells were placed into RPMI with 10% FBS. For transient transfections, cells were then grown for 48 hours. For the generation of stable cell lines, Geneticin (G418, Life Technologies) was added at a final concentration of 1mg/ml after 48 hours. After 2 weeks of culturing, cells stably transfected with Fes-GFP constructs were FACS sorted and the highly GFP-labeled cell population was expanded and maintained in Geneticin containing RPMI medium. RAW264.7 cells were cultured in Dulbecco's Modified Eagle's Medium supplemented with 10% FBS.

For BCR stimulation experiments, DG75 cells were starved using RPMI medium without FBS for 2 hours. For kinase inhibition, cells were incubated for 1 hour with respective kinase inhibitor (1uM final

concentration). Cells were pelleted and resuspended in 1ml of RPMI. Goat anti-human IgM was added at an amount of 1 microliter of a 10 mg/ml solution per 1 million cells. After incubation at 37°C, cells were put on ice, pelleted and frozen on dry ice prior to analysis.

Gateway cloning and Openfreezer repository

A detailed cloning summary is provided in Table S7 including acknowledgements of clones from external sources. To create gateway entry clones, Open Reading Frames (ORFs) were amplified by polymerase chain reaction (PCR) from the templates indicated in Table S7 using Phusion DNA polymerase (NEB) with Gateway compatible sequences appended to the end of the primers (5' sequence - gggg aca act ttg tac aaa aaa gtt ggc acc, 3' sequence - gggg ac aac ttt gta caa gaa agt tgg gta). The resulting products were then cloned into pDONR223 (*45*) using BP clonase (Invitrogen) and subsequently into Gateway destination vectors using LR Clonase (Invitrogen) according to the manufacturer's protocols. All inserts were sequence verified using CodonCode Aligner software. Clones were tracked in OpenFreezer (*46*). Point mutations were generated in relevant expression vectors using the QuikChange methodology according to the manufacturer's instructions (Agilent Technologies).

Immunofluorescence microscopy

DG75 cells were starved for 1 hour in RPMI without FBS causing adherence of the cells to glass cover slips. Cells were fixed with 2% paraformaldehyde in PBS for 10 minutes. Cells were washed 3 x 5 minutes with PBS. Permeabilization was performed by incubation with 0.5% Triton-X100 in PBS for 5 minutes. Cells were washed 3 x 5 minutes in PBS. Blocking was performed for 1 hour with 5% BSA and 0.1% Tween-100 in PBS. Primary antibody labeling was performed in 1% BSA using an anti-Fes antibody (Cell Signaling Technology) and goat anti-human IgM to label the B-cell receptor. Cells were

washed 3 x 5 minutes in PBS. Secondary labeling was performed using a donkey anti-rabbit Alexa Fluor 647 (Abcam) and a donkey anti-goat Alexa Fluor 488 (Abcam) in 1% PBS for 1 hour. The actin cytoskeleton was labeled simultaneously with Alexa Fluor 555 Phalloidin (Life Technologies). Cells were washed 3 x 5 minutes in PBS and cover slips were rinsed with water and mounted face down on glass slides. Samples were then imaged on an Inverted Leica DMIRE-2 microscope equipped with fluorescence optics. Using either a 60X- or 100X-oil immersion lens, fluorescent images were projected onto a Hamamatsu ORCA CCD camera and captured using VOLOCITY software (Improvision).

FSBA assisted kinase assays

5'-(4-Fluorosulfonylbenzoyl) adenosine hydrochloride (FSBA) was obtained from Sigma-Aldrich. $1x10^7$ DG75 cells were pelleted and lysed in NP40 buffer containing cOmplete, EDTA free protease inhibitor cocktail (Roche) by passing them through a 25-gauge needle and three pulses of sonication. Cell debris was removed by a 10000g centrifugation step for 10 minutes. Protein concentration was adjusted to 5mg/ml. FSBA was dissolved in DMSO (25mg FSBA in 500ul DMSO) and added to the cell lysate in a 1(FSBA):5 (lysate) ratio. The mixture was incubated at 30°C for 1 hour. DMSO was diluted to 5% with NP40 buffer and precipitated FSBA was removed by centrifugation for 2 minutes at 10000g. Sample volume was concentrated in YM-10 spin columns and adjusted to 3mg/ml. For the kinase assay, the kinase inhibited lysate was diluted 1:1 with 40mM MOPS, pH 7.2, 50mM glycerophosphate, 10mM EGTA, 2mM $NaVO_4$, 2mM DTT, 50mM $MgCl_2$, 2mM ATP. Purified kinase (full length Fes and SH2-kinase) was added (equal amount of activity) and assayed at 30°C for 30 min. 20ug of protein lysate was subsequently analyzed by blotting with anti-phosphotyrosine antibody (4G10).

Multiple reaction monitoring (MRM) mass spectrometry

Raw data files from data-dependent acquisition (DDA) experiments were imported into MRMpilot 1.1 (SCIEX) software to generate a list of potential sMRM transitions. Peptide retention times were determined by MS/MS from multiple MRM Initiated Detection and Sequencing (MIDAS) analyses using MultiQuant (version 2.1) software. The final sMRM method consisted of 54 transitions from the Fes kinase. For data normalization, we chose 5 Fes peptides that were unlikely to undergo post-translational modifications. sMRM analysis was performed on a hybrid triple quadrupole/ion trap mass spectrometer (5500 QTrap; SCIEX). Chromatographic separation of peptides was carried out on a nano-LC system (Eksigent, Dublin CA) coupled to a 100 μm i.d. fused silica column packed with 5μm ReproSil-Pur C18-AQ as a trap column and a 75 μm i.d. fused silica column packed with 3 μm Reprosil-Pur C18-AQ as the separation column (pulled to ~ 10 μM) to act as an electrospray emitter. Peptides were separated with a linear gradient from 2-30% acetonitrile in 90 min at a flow rate of 300nl/min. The MIDAS workflow was employed for sMRM transition confirmation. Each sMRM run was scheduled using previously determined LC retention times with a 5-minute MRM detection window and a 3-second scan time with both Q1 and Q3 settings at unit resolution. The MS/MS spectra acquired by MIDAS were first searched against relevant Ensembl databases using Mascot to confirm the identities of peptides. Then the raw data was imported into MultiQuant v2.1 (SCIEX) for automatic MRM transition detection followed by manual inspection by the investigators to increase confidence. Subsequently, the extracted Ion Chromatogram (XIC; proportional to peptide abundance) of each transition was calculated.

Cell lysis and dimethyl labeling

DG75 cell pellets were frozen on dry ice. Cells were lysed in 50mM ammonium bicarbonate, 8M urea, EDTA free cOmplete protease inhibitor cocktail (Roche), 2mM vanadate, phosphatase inhibitor cocktail 3 (Sigma-Aldrich). Three 20s pulses of sonication were used to solubilise the material. Proteins were reduced by the addition of dithiothreitol (final concentration of 20mM) for 30 min at room temperature.

Alkylation was performed by adding iodoacetamide (50mM final concentration) and incubation for 30 min. Urea concentration was subsequently reduced to 2M and proteins were digested overnight at 37°C after the addition of trypsin (Sigma-Aldrich) at a 1:100 ratio. A second round of digestion was performed for 2 hours. Samples were acidified with formic acid (5% final volume) and forming precipitate was removed by centrifugation. Peptides were bound on C18 Sep Pak cartridges (Waters) and desalted with 5% formic acid. Chemical dimethyl labeling was performed on column (*47*). Samples were combined after elution and freeze dried.

Phosphopeptide analysis

90mg of dried combined peptide sample was split into two equal batches. With the first batch, immunoprecipitation of tyrosine phosphorylated peptides was carried out. Peptides were dissolved in 5ml IP buffer (50mM Tris, pH 7.4, 150mM NaCl, 0.6% NP-40). 80ul of anti-phosphotyrosine (4G10) agarose beads (Millipore) were added and incubated for 2 hours. Beads were subsequently washed three times with IP buffer and 3 times with water. Peptides were eluted two sequential times with 0.2% TFA and the eluates were combined and freeze dried before mass spectrometry analysis.

The second batch was dissolved in 0.3% TFA, 25% lactic acid, 60% acetonitrile. Titansphere TiO_2 material (GL Science) was added in a peptide to TiO2 ratio of 1:6 and phosphopeptides were enriched according to the Titansphere manual instructions. After sequential elutions with 1% ammonia and 1% pyrrolidine, eluates were combined and the solvent evaporated. A desalting step using Sep Pak columns (Waters) was performed before the phosphopeptides were freeze dried and reconstituted in 30% acetonitrile, 5mM KH_2PO_4, pH 2.7. Peptide fractionation was carried out using a PolySULFOETHYL A column (PolyLC inc.), (*48*). Two minute fractions were collected until 60 min and subsequently freeze dried. Desalting of the fraction was carried out using C18 stage tips (Thermo Scientific) according to the stage tip description. The organic eluent solvent was evaporated and fractions were analyzed on a

Orbitrap Velos mass spectrometer coupled to a 1D+ Nano LC (Eksigent). Samples were injected directly onto a column packed in-house (75 μm inner diameter) with 3.5 μm Zorbax C-18 (Agilent) and analyzed using a 90 min gradient from 5%-30% solvent B (Solvent A: 0.1% formic acid in water; Solvent B: 0.1% formic acid in acetonitrile) at a flow rate of 250 nl/min. Raw data was processed using MaxQuant v.1.1.1.36. Mass tolerance for the first search was set to 20ppm. Oxidation (M) and phospho (S/T/Y) were set as variable modifications while Caramidomethyl (C) was set as fixed modification. Peptide and site false discovery rate were set to 0.01. All other settings were kept as default. Data was searched against the human Refseq database v.42 (*49*) and the obtained phosphopeptide evidence (Table S1) was subjected to SELPHI analysis. The mass spectrometry proteomics data have been deposited to the ProteomeXchange Consortium via the PRIDE partner repository (*50*) with the dataset identifier PXD005332 (username: reviewer47219@ebi.ac.uk; password: w1BLTp6y).

SELPHI analysis

Replicate sample and conditions were merged by keeping the ratio that indicated the maximum level of change in the phospho-peptide intensity. The protein sequences on which the peptide locations were mapped were extracted from the Human RefSeqV42 (*49*) and the gene names were mapped using UniprotKB release 2014_09 (*51*). We restricted the dataset to peptides that appear in at least six conditions, i.e. 2 samples and we applied a SELPHI-analysis (*15*) using the default parameters (Spearman correlation cutoff = 0.5 and p-value of correlation 0.05) on the combined datasets. SELPHI identified pairs of kinases associated with the identified phospho-peptides (Tables S2/3).

Fes kinase purification

cDNAs encoding human Fes (NP_001996) were cloned into pNIC28-Bsa4. Expression constructs were transformed into phage-resistant *E. coli* BL21(DE3)-R3 co-transformed with an expression vector encoding *Yersinia* phosphatase YopH. Cells were grown and Fes SH2-kinase proteins were purified according to previously described procedures (*30*).

Peptide array and radioactive kinase assays

Peptide arrays were prepared using an automated Multipep synthesizer (Intavis) on a cellulose support with standard F-moc chemistry protocols as recommended by the manufacturer and previously described (Warner et al., 2008). Prior to the kinase assay, the membranes were conditioned through a first rinse in 95% EtOH followed by the washing steps, 3x 5 min with TBS-T (20 mM Tris HCl, pH 7.5, 150 mM NaCl, 0.05% Tween 20), 2x 5 min with TBS (20 mM Tris HCl, pH 7.5, 150 mM NaCl) and 2x 5 min with kinase reaction buffer (KRB – 250 mM NaCl, 20 mM MgCl2, 20 mM MnCl2 in 50 mM HEPES buffer pH 7.5). For the kinase reaction, 50 μg of purified Fes SH2-kinase was used in 5 mL of KRB containing 50 μCi of radio-labeled γ32P-ATP and 40 μM unlabelled ATP. The reaction was stopped by three 20 min washes in Wash Buffer A (8M urea, 1% SDS, 0.5% beta-mercaptoethanol) followed by one 20 min wash in Wash Buffer B (50% EtOH, 10% acetic acid). The membrane was rinsed in 95% EtOH and allowed to air dry prior to exposing XAR film (Kodak) (*52*).

Immunoprecipitation and MS analysis of protein complexes

DG75 cells were transiently transfected with Gateway expression vectors (Invitrogen) containing GFP tagged Dok1, Sts1 and Ptpn18 constructs. At the same time a flag-tagged Fes E708A gain-of-function construct was also transfected. 48 h after transfection, cells were harvested, stimulated or not for 10 minutes with goat anti-human IgM and lysed in NP-40 buffer. Protein complexes were

immunoprecipitated using GFP-Trap (Chromotek) and washed 3 times with 50mM ammonium bicarbonate after the precipitation to remove detergent. Samples were processed using a solid-phase digest protocol as previously described (*53*). Briefly, columns were made with 200 μm (internal diameter) fused-silica tubing and packed with 3 cm of PolySulphoethyl A beads (particle size 12 μm, pore size 300 Å) (Western Analytical, CA, USA) using a pressure bomb (nitrogen gas, 100-500 psi). Protein eluates were loaded on the column and washed with 10 mM potassium phosphate buffer pH 3 followed by HPLC grade water. Bound proteins were reduced in DTT solution (100 mM DTT/10 mM NH_4HCO_3, pH 8) for 30 minutes and washed with HPLC grade water. Reduced proteins were alkylated and trypsin-digested for 1-2 hours in trypsin solution (2 mg/ml sequencing grade porcine trypsin (Promega)/100 mM Tris/10 mM iodoacetamide, pH 8). Peptides were eluted in 15 μl of 200 μM NH_4HCO_3, pH 8 and 1 μl of 50% formic acid was added for a final volume of 16 μl. Samples were analyzed on a TripleTOF 5600 mass spectrometer equipped with a nanospray III ion source (AB SCIEX), and coupled to a 1D+ Nano Ultra LC (Eksigent). Samples were injected directly onto a column packed in-house (75 μm inner diameter) with 3.5 μm Zorbax C-18 (Agilent) and analyzed using a 90 min gradient from 5%-30% solvent B (Solvent A: 0.1% formic acid in water; Solvent B: 0.1% formic acid in acetonitrile) at a flow rate of 250 nl/min. Tandem mass spectra were extracted, charge state deconvoluted and deisotoped in Analyst version 2.0. Wiff files were converted to .mgf format using ProteinPilot software and both formats were stored in ProHits (*54*). All MS/MS spectra were analyzed using Mascot (Matrix Science) version 2.2 against the human RefSeq database (release 57 supplemented with entries from the cRAP database from GPM - a total of 72226 sequences; 39792614 residues). Trypsin was chosen for digestion with up to 2 missed cleavages. Carbamidomethyl (C) was set as a fixed modification and oxidation (M), Phospho (ST) and Phospho (Y) were set as a variable modification. ESI-QUAD-Tof type fragmentation was selected with peptide mass tolerance set to 30 ppm, and fragment mass tolerance set to 0.2 Da (peptide identifications in Table S5).

We first extracted the total peptide counts for each identified protein and generated files compatible with SAINT (*55*). The preys were also annotated with the score from the CRAPome database (*56*). We only consider as interactors preys with a SAINT score greater than 0.8 (SAINT output can be found in Table S6).

Csk binding and phosphorylation assays

Mammalian expression vectors encoding Flag-epitope tagged full-length Csk and eGFP-tagged Ptpn18 WT & Y/F mutant were transfected into 293T cells using 5 ug/mL PEI (Polyethylenimine, Sigma Aldrich) in Opti-MEM (GIBCO). Following 18-hour transfection, cells were stimulated with hydrogen peroxide-activated sodium vanadate for 15 min at 37°C. Lysates, prepared in 50 mM Tris HCl pH 7.5, 150 mM NaCl, 3 mM EDTA, 1 % NP40, 10 ug/mL aprotinin, 10 ug/mL leupeptin, 1 mM Na Vanadate, were proportioned for analysis of protein expression (5%) and immunoprecipitation (95%) using GFP-Trap beads (ChromoTek, Germany). Co-immunoprecipitated proteins were detected using anti-Flag antibody (M2 – Sigma), eGFP fusion protein levels monitored using anti-GFP antibody (ab290 – abcam) and phosphotyrosine levels by blotting with anti-phosphotyrosine antibody (4G10) and ECL visualization.

Western blot

Protein blots were produced by semidry transfer. Visualization of antibody signals was achieved using HRP-conjugated secondary antibodies and the chemiluminescence substrate SuperSignal West Pico (Thermo Fisher Scientific). Blots were imaged and quantitatively analyzed using a Chemidoc MP imager (Biorad). *In-vitro* kinase assays for Sts1, Dok1, Ptpn18 and Cttn were evaluated using an Odyssey

Infrared Imaging System (LI-COR) using fluorescently labeled secondary antibodies at 800nm and 680nm. Images were analyzed using the ImageJ software (http://imagej.nih.gov/ij/).

Inhibitors and antibodies

Src Inhibitor 1, PP2 and PD184352 were obtained from Sigma Aldrich. The TAE684 compound was obtained from the Gray laboratory (Harvard Medical School, Boston).

Antibodies against the following proteins were obtained from Cell Signaling Technology:

Fes (#2736), Lyn (#2732), phospho-Lyn Y507 (#2731), phospho-Btk Y223 (#5082), phospho-Syk Y525/526 (#2711), CD19 (#3574), phospho-CD19 Y531 (#3571), Akt (#9272), phospho-Akt S473 (#9271), Erk1/2 (#9102), phospho-Erk1/2 (#9101), GFP (#2555), Src (#2108), phospho-Src Y527 (#2105),

Antibodies against the following proteins were obtained from Santa Cruz Biotechnology:

Fes (sc-7671), Dok1 (sc-6374), Gapdh (sc-365062)

Antibodies obtained from other vendors:

Anti-phosphotyrosine 4G10 (Millipore), anti-Flag M2 (Sigma Aldrich), goat anti-human IgM (Southern Biotech), anti-GFP ab290 (Abcam)

Author Contributions

AOH, TP, MK and KL conceived the study. AOH conducted most experiments and wrote the manuscript. MK performed kinase purifications and provided constructs. EP designed the Proteomics Pipeline. CZ and MT provided technical assistance to mass spectrometric analysis. GG synthesized the peptide arrays

and performed Csk binding assays. KC contributed to manuscript preparation and funding. TP provided funding, lab space and facilities.

Acknowledgements

This work was supported by the Ontario Research Fund Round 5 and GL2 grants to Dr. Tony Pawson and CIHR MOP 6849.

Bibliography

1. I. Sadowski, J. C. Stone, T. Pawson, A noncatalytic domain conserved among cytoplasmic protein-tyrosine kinases modifies the kinase function and transforming activity of Fujinami sarcoma virus P130gag-fps. *Mol. Cell. Biol.* **6**, 4396–408 (1986).
2. J. E. DeClue, I. Sadowski, G. S. Martin, T. Pawson, A conserved domain regulates interactions of the v-fps protein-tyrosine kinase with the host cell. *Proc. Natl. Acad. Sci. U. S. A.* **84**, 9064–8 (1987).
3. K. Tsujita *et al.*, Coordination between the actin cytoskeleton and membrane deformation by a novel membrane tubulation domain of PCH proteins is involved in endocytosis. *J. Cell Biol.* **172**, 269–79 (2006).
4. V. a McPherson *et al.*, Contributions of F-BAR and SH2 domains of Fes protein tyrosine kinase for coupling to the FcepsilonRI pathway in mast cells. *Mol. Cell. Biol.* **29**, 389–401 (2009).
5. P. Greer, Closing in on the biological functions of Fps/Fes and Fer. *Nat. Rev. Mol. Cell Biol.* **3**, 278–289 (2002).
6. S. a Parsons, P. a Greer, The Fps / Fes kinase regulates the inflammatory response to endotoxin through down-regulation of TLR4 , NF- B activation , and TNF- alpha secretion in macrophages regulation of innate immunity. *J. Leukoc. Biol.* (2006), doi:10.1189/jlb.0506350.1.
7. A. Carè *et al.*, c-fes expression in ontogenetic development and hematopoietic differentiation. *Oncogene*. **9**, 739–47 (1994).
8. J. Kim, R. a Feldman, Activated Fes Protein Tyrosine Kinase Induces Terminal Macrophage Differentiation of Myeloid Progenitors (U937 Cells) and Activation of the Transcription Factor PU . 1 Activated Fes Protein Tyrosine Kinase Induces Terminal Macrophage Differentiation of. *Mol. Cell. Biol.* **22**, 1903–1918 (2002).
9. I. MacDonald, J. Levy, T. Pawson, Expression of the mammalian c-fes protein in hematopoietic cells and identification of a distinct fes-related protein. *Mol. Cell. Biol.* **5**, 2543–51 (1985).
10. E. Voisset *et al.*, FES kinases are required for oncogenic FLT3 signaling. *Leuk. Off. J. Leuk. Soc. Am. Leuk. Res. Fund, U.K.* **24**, 721–728 (2010).
11. A. Bardelli, Mutational Analysis of the Tyrosine Kinome in Colorectal Cancers. *Science (80-.).* **300**,

949–949 (2003).

12. W. Sangrar *et al.*, An identity crisis for fps/fes: Oncogene or tumor suppressor? *Cancer Res.* **65**, 3518–3522 (2005).

13. B. Scheijen, J. D. Griffin, Tyrosine kinase oncogenes in normal hematopoiesis and hematological disease. *Oncogene*. **21**, 3314–33 (2002).

14. S. Hellwig *et al.*, Small-molecule inhibitors of the c-Fes protein-tyrosine kinase. *Chem. Biol.* **19**, 529–40 (2012).

15. E. Petsalaki *et al.*, SELPHI: correlation-based identification of kinase-associated networks from global phospho-proteomics data sets. *Nucleic Acids Res.* (2015), doi:10.1093/nar/gkv459.

16. R. L. Geahlen, Syk and pTyr'd: Signaling through the B cell antigen receptor. *Biochim. Biophys. Acta - Mol. Cell Res.* **1793** (2009), pp. 1115–1127.

17. F. Sacco *et al.*, Tumor suppressor density-enhanced phosphatase-1 (DEP-1) inhibits the RAS pathway by direct dephosphorylation of ERK1/2 kinases. *J. Biol. Chem.* **284**, 22048–22058 (2009).

18. A. Alexa *et al.*, Structural assembly of the signaling competent ERK2-RSK1 heterodimeric protein kinase complex. *Proc. Natl. Acad. Sci. U. S. A.* **112**, 2711–6 (2015).

19. Z. Songyang *et al.*, Specific motifs recognized by the SH2 domains of Csk, 3BP2, fps/fes, GRB-2, HCP, SHC, Syk, and Vav. *Mol. Cell. Biol.* **14**, 2777–2785 (1994).

20. D. C. Otero, S. A. Omori, R. C. Rickert, Cd19-dependent activation of Akt kinase in B-lymphocytes. *J. Biol. Chem.* **276**, 1474–8 (2001).

21. D. Depoil *et al.*, CD19 is essential for B cell activation by promoting B cell receptor-antigen microcluster formation in response to membrane-bound ligand. *Nat. Immunol.* **9**, 63–72 (2008).

22. K. B. Kaplan *et al.*, Association of the amino-terminal half of c-Src with focal adhesions alters their properties and is regulated by phosphorylation of tyrosine 527. *EMBO J.* **13**, 4745–56 (1994).

23. W. T. Miller, Tyrosine kinase signaling and the emergence of multicellularity. *Biochim. Biophys. Acta*. **1823**, 1053–7 (2012).

24. R. B. Irby, T. J. Yeatman, Role of Src expression and activation in human cancer. *Oncogene*. **19**, 5636–42 (2000).

25. E. K. Greuber, P. Smith-Pearson, J. Wang, A. M. Pendergast, Role of ABL family kinases in cancer: from leukaemia to solid tumours. *Nat. Rev. Cancer*. **13**, 559–71 (2013).

26. J. B. Casaletto, A. I. McClatchey, Spatial regulation of receptor tyrosine kinases in development and cancer. *Nat. Rev. Cancer*. **12**, 387–400 (2012).

27. N. Gupta, A. L. DeFranco, Lipid rafts and B cell signaling. *Semin. Cell Dev. Biol.* **18**, 616–626 (2007).

28. C. A. Koch, M. Moran, I. Sadowski, T. Pawson, The common src homology region 2 domain of cytoplasmic signaling proteins is a positive effector of v-fps tyrosine kinase function. *Mol. Cell. Biol.* **9**, 4131–40 (1989).

29. G. Weinmaster, T. Pawson, Localization and characterization of phosphorylation sites of the Fujinami avian sarcoma virus and PRCII virus transforming proteins. *J. Cell. Biochem.* **20**, 337–48 (1982).

30. P. Filippakopoulos *et al.*, Structural coupling of SH2-kinase domains links Fes and Abl substrate recognition and kinase activation. *Cell*. **134**, 793–803 (2008).

31. K. Kowanetz *et al.*, Suppressors of T-cell receptor signaling Sts-1 and Sts-2 bind to Cbl and inhibit endocytosis of receptor tyrosine kinases. *J. Biol. Chem.* **279**, 32786–95 (2004).

32. Z. Songyang, Y. Yamanashi, D. Liu, D. Baltimore, Domain-dependent Function of the rasGAP-binding Protein p62Dok in Cell Signaling. *J. Biol. Chem.* **276**, 2459–2465 (2001).

33. T. Vang, H. Abrahamsen, S. Myklebust, V. Horejsí, K. Taskén, Combined spatial and enzymatic regulation of Csk by cAMP and protein kinase a inhibits T cell receptor signaling. *J. Biol. Chem.* **278**, 17597–600 (2003).

34. P. Filippakopoulos, S. Müller, S. Knapp, SH2 domains: modulators of nonreceptor tyrosine kinase activity. *Curr. Opin. Struct. Biol.* **19** (2009), pp. 643–649.

35. H. Huang *et al.*, Defining the specificity space of the human SRC homology 2 domain. *Mol. Cell. Proteomics*. **7**, 768–784 (2008).

36. J. Raguz, S. Wagner, I. Dikic, D. Hoeller, Suppressor of T-cell receptor signalling 1 and 2 differentially regulate endocytosis and signalling of receptor tyrosine kinases. *FEBS Lett.* **581**, 4767–72 (2007).

37. A. Mikhailik *et al.*, A phosphatase activity of Sts-1 contributes to the suppression of TCR signaling. *Mol. Cell*. **27**, 486–97 (2007).

38. M. Beckwith, G. Jorgensen, D. L. Longo, The protein product of the proto-oncogene c-cbl forms a complex with phosphatidylinositol 3-kinase p85 and CD19 in anti-IgM-stimulated human B-lymphoma cells. *Blood*. **88**, 3502–7 (1996).

39. M. S. Mahmoud, R. Fujii, H. Ishikawa, M. M. Kawano, Enforced CD19 expression leads to growth inhibition and reduced tumorigenicity. *Blood*. **94**, 3551–3558 (1999).

40. G. Mateo *et al.*, Prognostic value of immunophenotyping in multiple myeloma: a study by the PETHEMA/GEM cooperative study groups on patients uniformly treated with high-dose therapy. *J. Clin. Oncol.* **26**, 2737–44 (2008).

41. E. Cannizzo *et al.*, The role of CD19 and CD27 in the diagnosis of multiple myeloma by flow cytometry: a new statistical model. *Am. J. Clin. Pathol.* **137**, 377–86 (2012).

42. R. E. Tiedemann *et al.*, Kinome-wide RNAi studies in human multiple myeloma identify vulnerable kinase targets, including a lymphoid-restricted kinase, GRK6. *Blood*. **115**, 1594–604 (2010).

43. J. Chen, A. Elfiky, M. Han, C. Chen, M. W. Saif, The role of Src in colon cancer and its therapeutic implications. *Clin. Colorectal Cancer*. **13**, 5–13 (2014).

44. M. J. Begley *et al.*, EGF-receptor specificity for phosphotyrosine-primed substrates provides signal integration with Src. *Nat. Struct. Mol. Biol.* (2015), doi:10.1038/nsmb.3117.

45. J.-F. Rual *et al.*, Human ORFeome version 1.1: a platform for reverse proteomics. *Genome Res.* **14**, 2128–35 (2004).

46. M. Olhovsky *et al.*, OpenFreezer: a reagent information management software system. *Nat. Methods*. **8**, 612–3 (2011).

47. P. J. Boersema, R. Raijmakers, S. Lemeer, S. Mohammed, A. J. R. Heck, Multiplex peptide stable isotope dimethyl labeling for quantitative proteomics. *Nat. Protoc.* **4**, 484–494 (2009).

48. S. Gauci *et al.*, Lys-N and trypsin cover complementary parts of the phosphoproteome in a refined SCX-based approach. *Anal. Chem.* **81**, 4493–4501 (2009).

49. K. D. Pruitt *et al.*, RefSeq: an update on mammalian reference sequences. *Nucleic Acids Res.* **42**,

D756-63 (2014).

50. J. A. Vizcaino *et al.*, 2016 update of the PRIDE database and its related tools. *Nucleic Acids Res.* **44**, D447–D456 (2016).

51. UniProt Consortium, UniProt: a hub for protein information. *Nucleic Acids Res.* **43**, D204-12 (2014).

52. N. Warner, L. E. Wybenga-Groot, T. Pawson, Analysis of EphA4 receptor tyrosine kinase substrate specificity using peptide-based arrays. *FEBS J.* **275**, 2561–73 (2008).

53. N. Bisson *et al.*, Selected reaction monitoring mass spectrometry reveals the dynamics of signaling through the GRB2 adaptor. *Nat. Biotechnol.* **29**, 653–8 (2011).

54. G. Liu *et al.*, ProHits: integrated software for mass spectrometry-based interaction proteomics. *Nat. Biotechnol.* **28**, 1015–7 (2010).

55. H. Choi *et al.*, *Curr. Protoc. Bioinformatics*, in press, doi:10.1002/0471250953.bi0815s39.

56. D. Mellacheruvu *et al.*, The CRAPome: a contaminant repository for affinity purification-mass spectrometry data. *Nat. Methods*. **10**, 730–6 (2013).

57. N. Colaert, K. Helsens, L. Martens, J. Vandekerckhove, K. Gevaert, Improved visualization of protein consensus sequences by iceLogo. *Nat. Methods*. **6**, 786–7 (2009).

Figure legends

Figure 1, The Fes kinase is an active signaling component in B-lymphocytes

(A) Immunofluorescence microscopy showing co-localization of endogenous Fes kinase with the B-cell receptor in fixed DG75 cells. (B) Schematic representation of the engagement of major B-cell receptor (BCR) signaling components, following receptor clustering after antigen binding. Src family kinase Lyn becomes activated recruiting downstream tyrosine kinases such as Syk to receptor signaling complexes. Following this, there is an activation of the MAP kinase cascade as well as recruitment of PI3K to the membrane and activation of Akt signaling. (C) Phosphoproteomic analysis of DG75 lysates showed that endogenous Fes kinase autophosphorylation on Y713 is increased following BCR stimulation for 10 minutes (+IgM). Intensities of the auto phosphorylated peptide (pY713) were normalized to five unmodified peptides from the SH2 and kinase domain. Samples were compared using dimethyl labeling. The compound TAE684 (1uM final concentration) was used to inhibit Fes kinase activity. (D) Multiple reaction monitoring (MRM) mass spectrometry analysis of the Fes auto-phosphorylation site during BCR

cross linking. DG75 cells were stably transfected with GFP-tagged full length Fes or an SH2-kinase version lacking the F-BAR domain. Both constructs were expressed at similar levels. Intensities of the auto phosphorylated peptide (pY713) were normalized to five unmodified peptides from the SH2 and kinase domain. (E) Western blot analysis, using an anti-phosphotyrosine antibody (4G10), of kinase assays on whole cell lysates was performed. DG75 cell lysate was rendered kinase-dead in advance by a broad spectrum kinase inhibitor (FSBA) treatment. Following this, equal amounts of Fes kinase activity were added for the respective kinases as measured by amount of kinase autophosphorylation (indicated by arrow). In lane 1, purified Fes SH2-kinase was added. Lane 2 was treated with the full-length Fes protein. Lane 3 contained inhibited lysate without added kinase. Lane 4 contained uninhibited cell lysate subjected to kinase assay conditions.

Figure 2, Analytical strategy reveals global signaling events and kinase substrate associations

(A) Table of phosphoproteomic experiments performed on the DG75 lymphocyte cell line. Kinase signaling pathways were perturbed by the stable or transient integration of exogenous wildtype Fes kinase as well as a gain of function kinase variant (E708A). Cells were stimulated by IgM cross linking for 5 or 20 minutes as indicated. Additional large-scale experiments evaluated the impact of Fes, Src and Mek inhibitors on signaling events. (B) After tryptic digestion and C18 peptide purification, peptides were labeled using chemical dimethyl labeling and phosphorylated peptides were isolated using TiO2 enrichment as well as anti-phosphotyrosine immunoprecipitation. TiO2 eluates were subsequently fractionated using strong cation exchange chromatography. Mass spectrometric analysis using an Orbitrap elite was followed by Maxquant data analysis (Table S1). Data integration and correlative analysis was performed using the SELPHI platform. This procedure allowed us to construct maps for potential kinase-substrate associations (Table S2/S3). In particular, tyrosine phosphorylation events were used to build

peptide arrays that were subsequently probed with purified Fes kinase to validate the bioinformatics results (Table S4). (C) Heatmap showing tyrosine kinase – substrate relationships. Correlation of phosphorylation site behavior was performed using SELPHI on the combined phosphoproteomics experiment data. Soluble tyrosine kinases (known kinase activating phosphorylation sites are marked with a star) are listed at the top and potential substrates on the left. Positive correlation is indicated in blue while negative correlations are shown in red.

Figure 3, Fes substrates and influence on B-cell kinase signaling networks

(A) Representative examples for radio kinase assays conducted on spots blots of synthesized peptides corresponding to 100 sites that were found to exhibit correlations with activating sites on soluble tyrosine kinases according to the SELPHI analysis. Phosphorylation profiles for purified Fes SH2-kinase and kinase domain alone were obtained using Icelogo (*57*) (Data in Table S4). (B) Amount of tyrosine phosphorylation in our peptide array of 13 SELPHI-identified Fes substrate sites compared to known Fes phosphorylation sites (positive controls, CTTN Y421 and Fes Y713 autophosphorylation site, are indicated in grey). Phosphorylation cutoff is indicated by the dashed line. (C) Tyrosine kinases that were found to be activated following BCR stimulation are depicted. Tyrosine phosphorylation sites that are described to affect kinase activity are marked by a star. Red connections symbolize kinase–substrate connections of the Fes kinase that were identified by SELPHI and confirmed via the peptide array. (D) A schematic showing the flow of kinase signaling based on our SELPHI analysis, indicating that Fes is capable of influencing kinase components of the phosphotyrosine signaling network (arrows) but is not directly manipulating components of the Tyrosine kinase – Serine/Threonine kinase interface or downstream kinase network (S/T kinase – substrate connection data in Table S3). (E) Non-kinase proteins that were found to be Fes substrates are depicted with the particular phosphorylation site indicated. Sts1, Ptpn18 and Dok1 are circled as they were used for further IP-MS experiments. (F) *In-vitro*

phosphorylation of Dok1, Sts1 and Ptpn18 (and their Y-to-F substituted counterparts) by purified Fes kinase. GFP-tagged proteins were expressed in DG75 cells, immunoprecipitated and phosphorylated using purified Fes SH2-kinase for 10 minutes. Kinase reaction was analyzed by immunoblotting (4G10) to assess the phosphorylation state.

Figure 4, Dynamic interactome analysis reveals Fes-mediated Csk recruitment

(A) Y-to-F substitutions of Fes phosphorylation sites were employed to study the interactome of Dok1, Sts1 and Ptpn18, revealing Y-F (Fes phosphorylation) dependent (orange) as well as Y-F independent and constitutive interactors (grey). Arrows towards the bait indicate association and arrows away from the bait disassociation following 10 minute BCR stimulation. Identified peptides for the respective baits are reported in Table S5. (B) Ion intensities of endogenous Sts1 pY19, Ptpn18 pY338 and Dok1 pY449 tyrosine-phosphorylated peptides in resting DG75 cells and following BCR cross-linking using anti-human IgM. The peptides were labeled using dimethyl labeling and Fes phosphorylation was inhibited using a pre-treatment with the TAE684 compound. (C) Co-expression of FLAG-tagged tyrosine kinases (Src, Fes, Fes E708A) with GFP-Ptpn18 showed that Fes but not Src is capable of causing Csk-Ptpn18 association. Mutation of Y388 to F (YF) on Ptpn18 abolished the interaction while the mutation of C228 to S (CS, phosphatase catalytic residue) did not affect Csk recruitment, double mutation indicated as D. (D) Co-transfection of Flag-Csk with GFP-Ptpn18 in Hek293T cells showed that expression of Csk leads to association with and phosphorylation of Ptpn18 which is dependent on Ptpn18 Y388. Either Csk is able to act on the same phosphorylation site as the Fes kinase (Y388) or it has to be recruited through Y388 before it can act on other tyrosine sites in Ptpn18.

Figure 5, Fes modulates CD19 protein levels via its substrate Sts1

(A) STRING (http://string-db.org/) protein association analysis performed on BCR components CD79A/B revealed a connection to Fes/Sts1/Csk directed signaling pathways via the E3 ubiquitin ligase Cbl. (B) Transient expression of Flag-tagged E708A Fes, Tec and Src in BCR-stimulated DG75 cells. Kinase expression levels were titrated (1, 5, 20, 50ug of plasmid DNA) while keeping the total amount of transfected DNA constant. * marks the exogenous Src protein while ** indicates endogenous Src. Protein levels, as indicated, were analyzed by immunoblotting. (C) GFP-tagged Dok1, Sts1 and Ptpn18 and their counterparts exhibiting mutations of the Fes phosphorylation sites were expressed in DG75 cells and stimulated with IgM. Effects on CD19 levels were analyzed by immunoblotting. (D) Fes signaling effects on CD19 protein abundance in B-lymphocytes. Exposure of the B-cell to low level exogenous Fes signaling increased endogenous CD19 abundance possibly by counteracting Cbl-mediated receptor degradation via the ubiquitin-binding tyrosine phosphatase Sts1 and its binding partner, the Src inhibiting tyrosine kinase Csk.

Figure S1

(A) Western blot analysis of endogenous Fes kinase from RAW684.3 (macrophage) and DG75 (B-lymphocyte) cell lines (Arrow indicates Fes protein band). Quantification of cellular protein levels is normalized to Gapdh and shown in the lower panel. (B) Western blot validation of activating phosphorylation sites on known BCR responders such as Syk, Btk, Lyn and CD19 showed a strong engagement of diverse signaling cascades following BCR stimulation of DG75 cells. (C) Downstream signaling pathways such as the recruitment of Akt to the membrane (Dok1 localization to the membrane is shown as a control for membrane preparations) and (D) activation of Akt and Erk pathways, as measured by phosphorylation of S473 and T202/Y204 respectively, confirmed DG75's suitability as a model system for BCR activation and signal processing.

Figure S2

(A) Evaluation of Cttn phosphorylation by the Fes SH2-kinase using co-expression and immunoblotting. Flag-tagged Cttn, Flag-tagged Fes SH2-kinase and Fes E708A SH2-kinase were transfected into DG75 cells and immunoprecipitated with Flag M2 antibody. Immunoblotting revealed increased autophosphorylation of Fes E708A as well as increased phosphorylation of the Cttn substrate as judged by anti-phosphotyrosine staining.

Figure S3

Heatmap showing serine/threonine kinase – substrate relationships. Correlation of phosphorylation site behavior was performed using SELPHI on the combined phosphoproteomics experiment data. Phosphorylation sites in serine/threonine kinases are listed at the top and potential associated substrates on the left. Positive correlation is indicated in blue while negative correlations are shown in red.

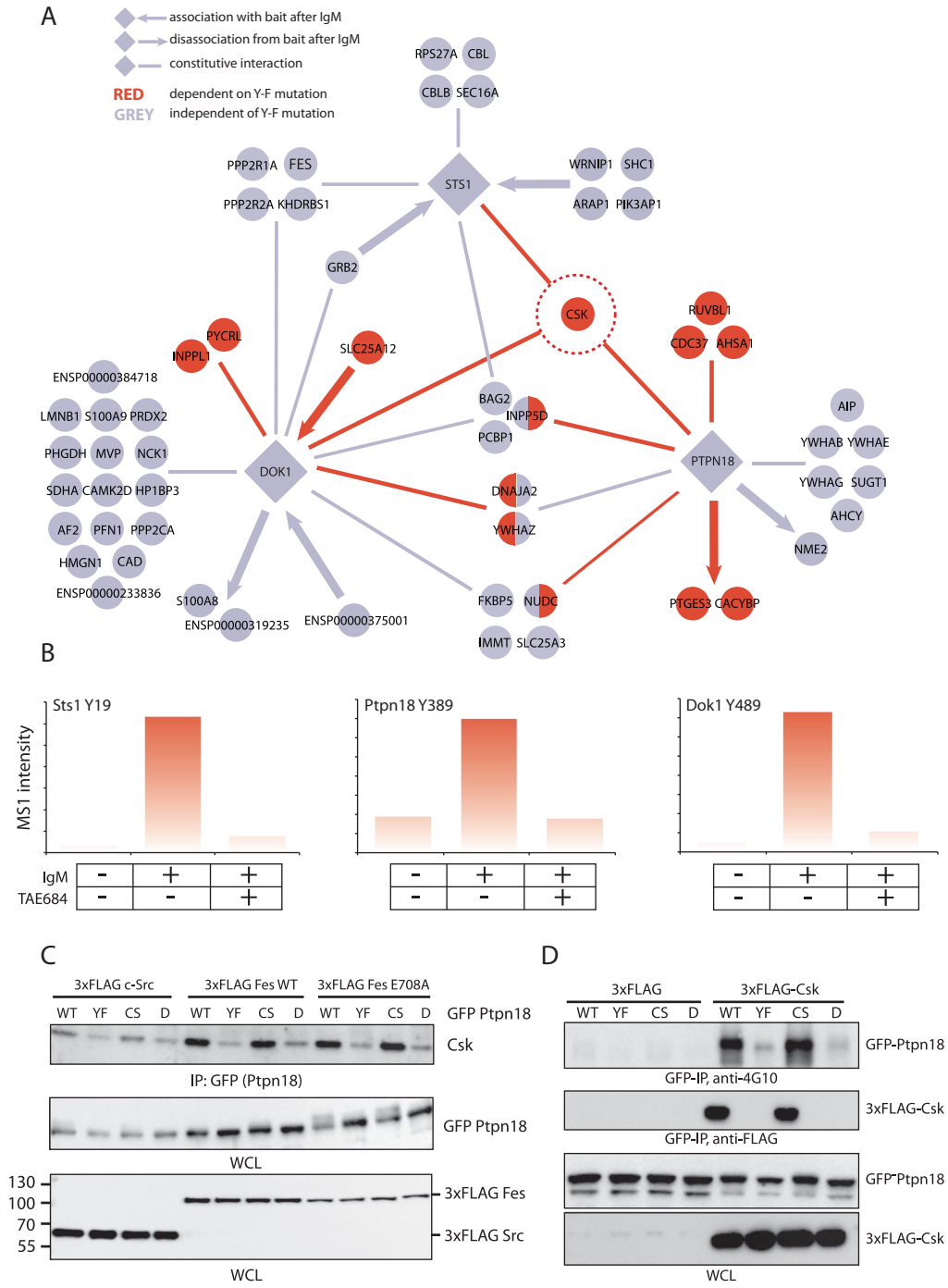

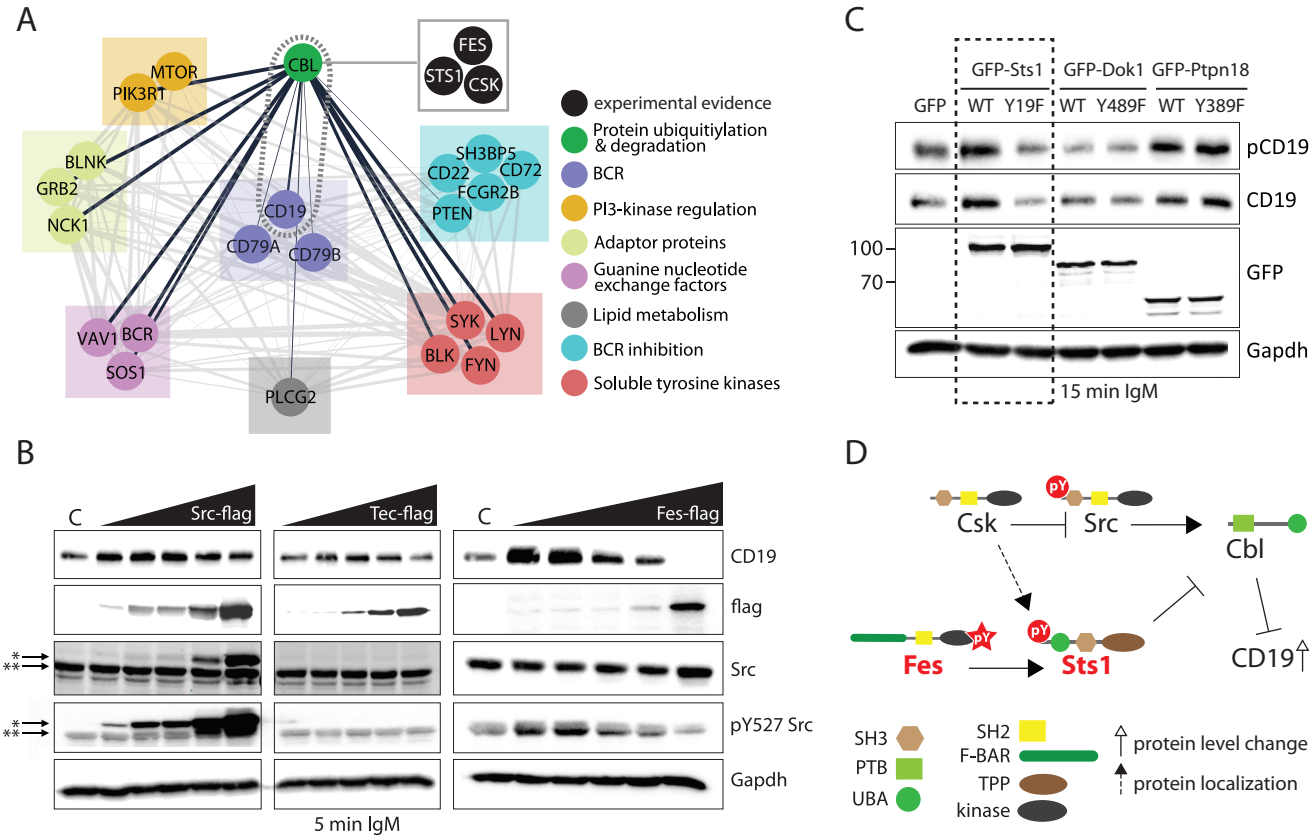

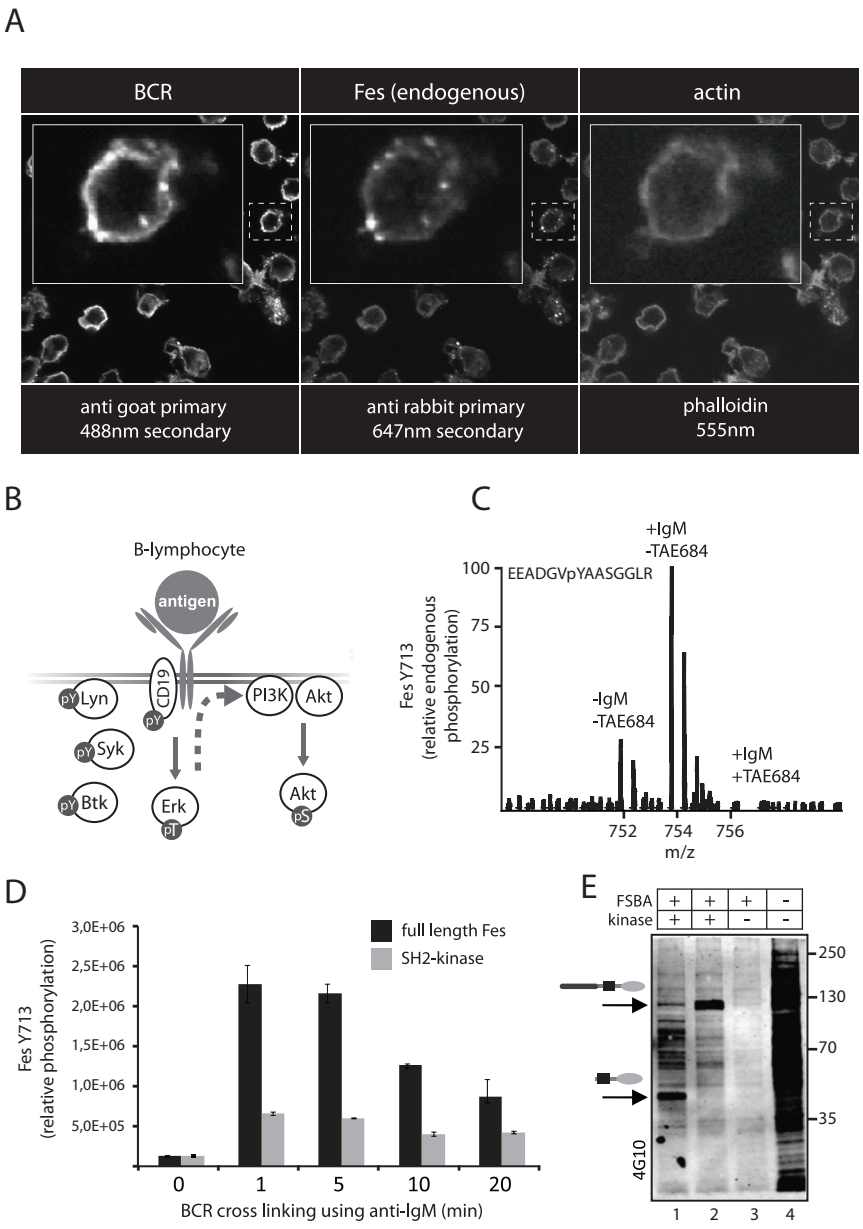

A

light (l)	medium (m)	heavy (h)
Fes expression level modulation		
GFP (s)	E708A Fes (s)	WT Fes (s)
GFP (t)	WT Fes (t)	E708A Fes (t)
IgM stimulation		
GFP (s)	E708A Fes (s)	E708A Fes (s) + 5min IgM
GFP (s)	E708A Fes (s)	E708A Fes (s) + 5min IgM
GFP (t) + 5min IgM	WT Fes (t) + 5min IgM	E708A Fes (t) + 5min IgM
IgM stimulation with kinase inhibitors		
DG75	DG75 + 5min IgM	DG75 + 5min IgM + TAE684
DG75	DG75 + 20min IgM	DG75 + 20min IgM + TAE684
DG75	DG75 + 20min IgM	DG75 + 20min IgM + TAE684
GFP (s)	GFP (s) + 20min IgM	GFP (s) + 20min IgM + TAE684
WT Fes (s)	WT Fes (s) + 5min IgM	WT Fes (s) + 5min IgM + TAE684
WT Fes (s)	WT Fes (s) + 20min IgM	WT Fes (s) + 20min IgM + TAE684
GFP (s) + 5min IgM	GFP (s) + 5min IgM + PP2	GFP (s) + 5min IgM + PD184352
WT Fes (s) Fes + 5min IgM	WT Fes (s) + 5min IgM + SrcI1	WT Fes (s) + 5min IgM + TAE684

(s) stable expression
(t) transient expression

B

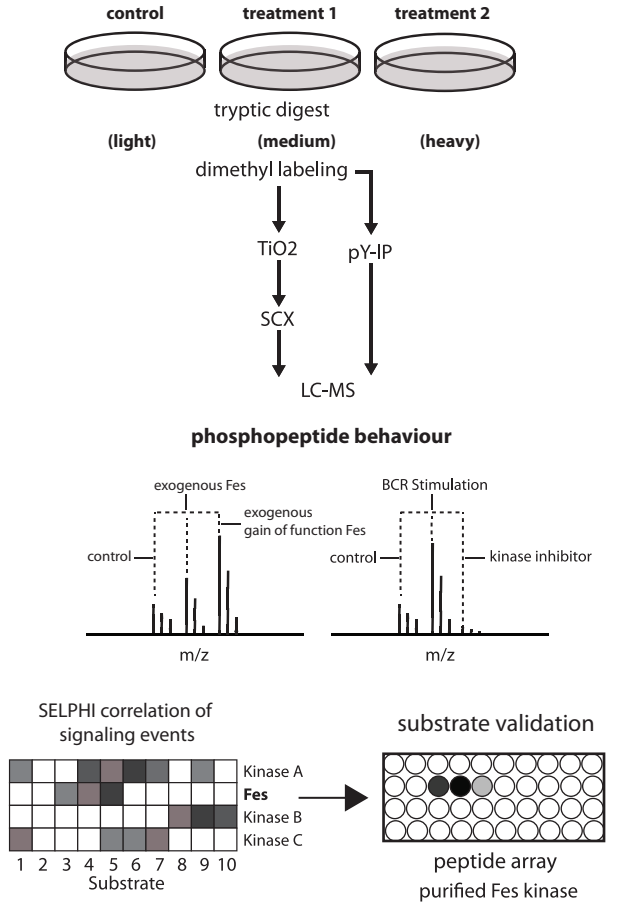

C